

# iMoWM: Taming Interactive Multi-Modal World Model for Robotic Manipulation

Chuanrui Zhang<sup>1</sup>, Zhengxian Wu<sup>2</sup>, Guanxing Lu<sup>2</sup>, Yansong Tang<sup>2</sup>, Ziwei Wang<sup>1</sup>

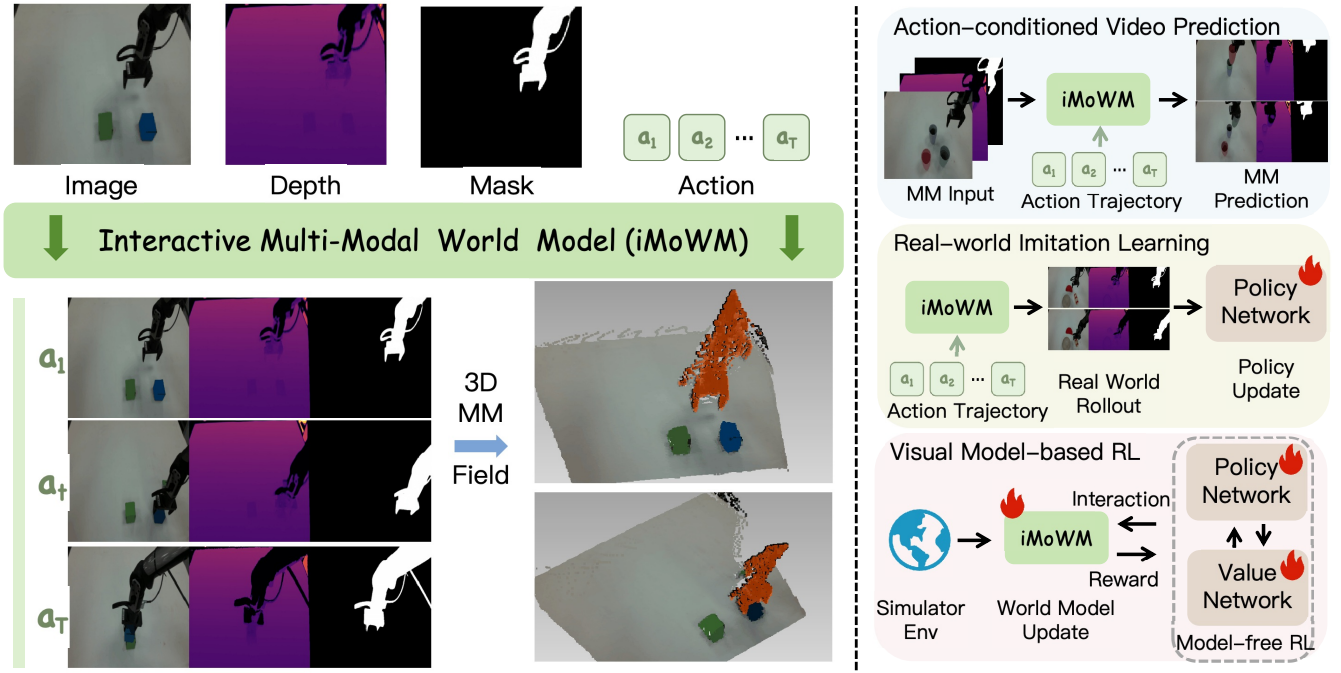


Fig. 1: Given color images, depth maps, and robot-arm masks, iMoWM generates future 3D multi-modal fields conditioned on actions. By incorporating geometric information, this multi-modal design enhances the representation of dynamic real-world scenes and improves the applicability of world models to robotic manipulation, supporting both real-world imitation learning and visual model-based reinforcement learning across diverse tasks.

**Abstract**—Learned world models hold significant potential for robotic manipulation, as they can serve as simulator for real-world interactions. While extensive progress has been made in 2D video-based world models, these approaches often lack geometric and spatial reasoning, which is essential for capturing the physical structure of the 3D world. To address this limitation, we introduce iMoWM, a novel interactive world model designed to generate color images, depth maps, and robot arm masks in an autoregressive manner conditioned on actions. To overcome the high computational cost associated with three-dimensional information, we propose MMTokenizer, which unifies multi-modal inputs into a compact token representation. This design enables iMoWM to leverage large-scale pretrained VideoGPT models while maintaining high efficiency and incorporating richer physical information. With its multi-modal representation, iMoWM not only improves the visual quality of future predictions but also serves as an effective simulator for model-based reinforcement learning (RL) and facilitates real-world imitation learning. Extensive experiments demonstrate the superiority of iMoWM across these tasks, showcasing the advantages of multi-modal world modeling for robotic manipulation. [Homepage: https://xingyoujun.github.io/imowm/](https://xingyoujun.github.io/imowm/)

## I. INTRODUCTION

In recent years, learned world models [1], [2] have been increasingly recognized as a promising paradigm, demonstrating substantial advances across a wide range of domains, including scene generation [3], [4], autonomous driving [5], [6], and gaming [7], [8]. By leveraging limited observations to generate anticipated future outcomes, these models exhibit a notable ability to predict world states under specific conditions while simultaneously facilitating adaptation to novel environments. These capabilities make learned world models particularly valuable for robotic manipulation [9], [10], where accurate prediction of physical dynamics during interaction is essential for efficient adaptation to diverse environments.

Some learned world models [11], [12] adopt a goal-conditioned framework, where text instructions are leveraged as conditioning signals. Building on large pre-trained video prediction models [13], [14], these approaches are capable of generating high-quality future video sequences. However, their applicability to robotic manipulation is limited, as they

<sup>1</sup>Nanyang Technological University, Singapore  
chuanrui001@e.ntu.edu.sg ziwei.wang@ntu.edu.sg

<sup>2</sup>Tsinghua University, Beijing, China

do not explicitly incorporate action sequences. Introducing action-based conditioning enables world models [12] to generate anticipated outcomes that correspond to each step in an action sequence, thereby better aligning predictions with embodied decision-making.

Despite this advancement, most recent methods [12], [15], [16] remain constrained to RGB video prediction and lack explicit 3D representations. This limitation is particularly critical for robotic manipulation, where actions unfold in three-dimensional space. Without sufficient geometric and spatial understanding, video-based world models are prone to errors under visual variations and complex object interactions. While GWM [9] attempts to overcome this by employing 3D Gaussian Splatting (3DGS) [17] for world representation, its effectiveness is highly dependent on the quality of the reconstructed 3DGS, making it unsuitable for monocular scenes and difficult to scale across diverse settings. Moreover, such 4D world models are computationally expensive to train and deploy, as they must represent both two-dimensional space and time. Consequently, how to efficiently represent and predict the dynamics of the 3D world remains an open challenge.

To address the aforementioned limitations, we propose **iMoWM**, a novel framework for an **interactive multi-modal world model**. iMoWM simultaneously predicts color images, depth maps, and robot arm masks, making it both geometry-aware and focused on dynamic robot arm. To reduce computational costs, we introduce MMTTokenizer, which encodes multi-modal inputs into a unified token representation. This module enables iMoWM to efficiently represent a 4D world model without incurring additional computational overhead. We then employ an autoregressive transformer framework to generate future 3D scenes in an interactively autoregressive manner with action-based condition. Thanks to this unified tokenization strategy, iMoWM can effectively leverage existing large-scale pretrained GPT models, such as iVideoGPT [12].

By virtue of its multi-modal design, iMoWM enhances the prediction of future 3D world states with improved visual fidelity, facilitates more effective real-world imitation learning, and provides a stable neural simulation framework for model-based reinforcement learning (RL). We evaluate iMoWM on both public benchmarks [18], [19], [20] and real-world datasets. Extensive experiments on action-conditioned video prediction, real-world imitation learning, and visual model-based RL demonstrate that iMoWM achieves state-of-the-art performance in terms of video quality and robotic manipulation success rate.

Comprehensively, our main contributions are as follows:

- We introduce iMoWM, a novel interactive world model that predicts color images, depth maps, and robot arm masks in an interactively autoregressive manner.
- iMoWM can generate videos for policy learning and serve as a simulator for reinforcement learning, demonstrating its strong potential for scalable robotic manipulation.
- iMoWM achieves the best performance in both visual

quality and robotic manipulation on public benchmarks and real-world experiments, demonstrating the effectiveness of multi-modal world modeling.

## II. RELATED WORK

### A. Learned World Models

Learning to predict future states of the observed world from action-based control inputs has long been a central challenge in domains such as autonomous driving [21], [6], [22], [23], game agents [7], [24], [25], [26], and robotic manipulation [27], [28], [29], [9]. Early approaches [12] are inspired by VideoGPT, where RGB video frames are tokenized and future color images are generated in an autoregressive manner. More recently, advances in diffusion-based video generation [13], [30], [14] have motivated world models [3], [31], [32] to predict future sequences within video latent spaces. Meanwhile, GWM [9] adopts 3D Gaussian Splatting (3DGS) as its underlying representation, however, limited pretraining data and the insufficient quality of 3DGS in monocular settings severely restrict its generative capacity on public datasets and real-world scenes. Nevertheless, improving 3D representation remains a critical prerequisite for advancing the applicability of learned world models to robotic manipulation.

### B. 4D Video Prediction

4D video generation [32], [33], [34] has attracted considerable attention in recent years, driven by advances in diffusion models and 3D Gaussian Splatting (3DGS) techniques. Previous approaches [9] utilize 3DGS to reconstruct the 3D geometry of generated videos, but these methods typically require multi-view consistent video generation, which limits their applicability to robotic manipulation. More recently, Tesseract [11] explores RGB-DN video generation, highlighting the importance of monocular 3D information for embodied tasks. Nonetheless, these approaches lack explicit action conditioning, which is essential for enhancing robotic manipulation performance.

### C. World Model for Robotic Manipulation

The primary objective of incorporating world models into robotic manipulation is to enrich real-world data for imitation learning in unseen scenarios [35], [36], [37], [38] and to serve as simulators for reinforcement learning (RL) [39], [40]. Previous approaches [9] have integrated world model observation encoders as feature extractors for imitation learning policies, which can largely be regarded as pretraining strategies. Other methods [12], [41] employ world models to support RL by reducing the high cost associated with constructing digital twins of the required environments. However, these approaches generally lack explicit 3D information, which limits their effectiveness both as simulators and as generators of realistic training data for real-world applications.

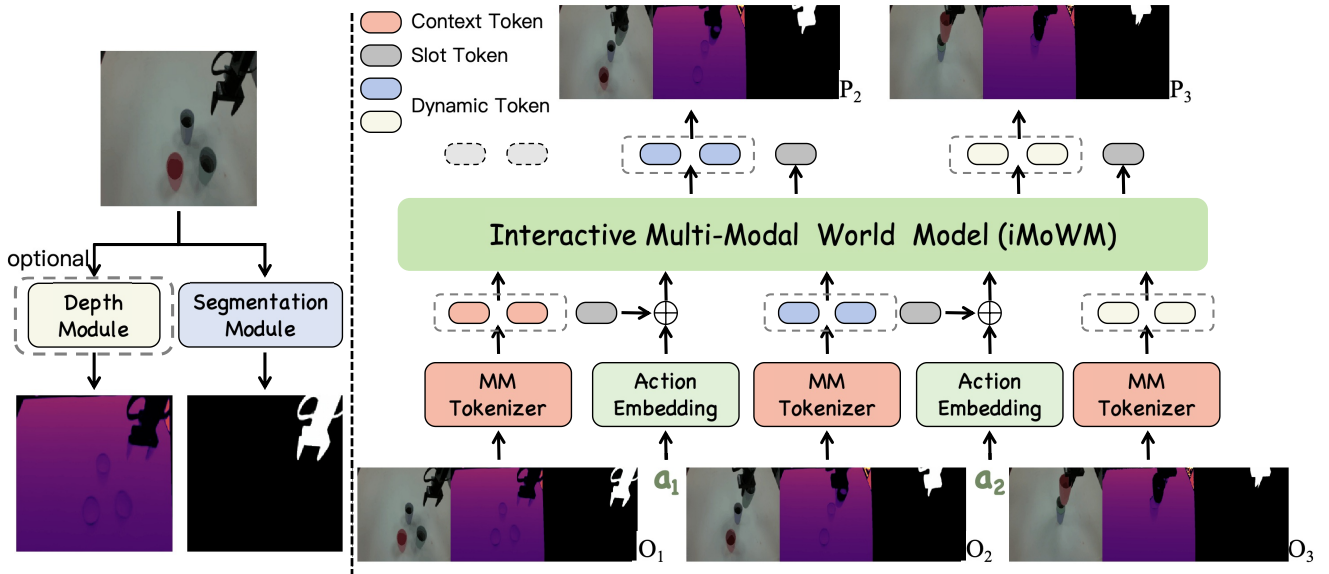


Fig. 2: **Framework of proposed iMoWM.** Our method takes a color image as input and extracts the robot-arm mask. The metric depth map is obtained either from RGB-D camera observations or from our depth module. These inputs are then encoded into discrete tokens using the proposed MMTokenizer. By injecting action-conditioned slot tokens, the autoregressive transformer generates future tokens sequentially, which are finally decoded into multi-modal outputs.

### III. METHOD

We introduce **iMoWM**, a novel multi-modal world model designed to predict future scenes with color images, depth maps, and robot arm masks. An overview of the proposed framework is presented in Figure 2. Given an initial color image input  $\mathbf{I}_1$ , we first generate its corresponding depth map and robot arm mask, which are then combined to form the multi-modal observation  $\mathbf{O}_1$ . This observation is processed by MMTokenizer, which encodes  $\mathbf{I}_1$  into a unified multi-modal token representation  $\mathbf{Z}_1$  (section III-A). An autoregressive transformer is then employed to predict subsequent tokens conditioned on the action sequence  $\{\mathbf{a}_t\}_{t=1}^T$  (section III-B). We demonstrate that iMoWM can be effectively applied to action-conditioned multi-modal video generation, real-world imitation learning, and model-based reinforcement learning for robotic manipulation tasks (section III-C).

#### A. MMTokenizer

Previous research has demonstrated the effectiveness of transformers in modeling sequences of discrete tokens [42], [43]. In the visual domain, VQGAN [44] has emerged as a widely adopted tokenizer that transforms pixel-level image representations into compact discrete tokens. Building on this foundation, and drawing inspiration from iVideoGPT [12], we employ a dual-encoder-decoder framework  $\{(\mathcal{E}_c, \mathcal{D}_c), (\mathcal{E}_d, \mathcal{D}_d)\}$ , which serves as a conditional VQGAN to directly tokenize video sequences. This design enables a more expressive representation of both contextual and dynamic information inherent in videos.

To extend this paradigm toward efficient multi-modal video processing, we propose MMTokenizer (shown in Figure 3). Specifically, we adapt the original encoders and

decoders  $\{(\mathcal{E}_c, \mathcal{D}_c), (\mathcal{E}_d, \mathcal{D}_d)\}$  into a unified multi-modal encoder-decoder architecture that can process and reconstruct multi-modal inputs as discrete tokens. Since the input now contains additional modalities beyond raw RGB frames (e.g., depth maps and segmentation masks), we replicate the first encoder layer and the final decoder layer to handle modality-specific feature distributions. Furthermore, to mitigate the different distribution across color images, depth signals, and mask representations, we introduce modality-specific embeddings that explicitly classify and guide the encoding and decoding processes for each modality. Through this design, MMTokenizer generates discrete multi-modal tokens suitable for transformer-based modeling, while maintaining comparable computational efficiency to standard video tokenization and achieving negligible performance degradation.

Utilizing the MMTokenizer, we employ a context encoder-decoder pair  $(\mathcal{E}_c, \mathcal{D}_c)$  to generate contextual tokens from the initial observations  $\mathbf{O}_{1:T_0}$ , where  $T_0$  denotes the number of context frames:

$$\mathbf{Z}_t^c = \mathcal{E}_c(\mathbf{O}_t), \quad \hat{\mathbf{O}}_t = \mathcal{D}_c(\mathbf{Z}_t^c) \quad t = 1, \dots, T_0. \quad (1)$$

In contrast, future frames often exhibit substantial temporal redundancy relative to the context frames, particularly in robotic manipulation scenarios, where only the robot arm and the interacted objects undergo significant changes. To exploit this property, we introduce a conditional encoder-decoder  $(\mathcal{E}_p, \mathcal{D}_p)$ , which focuses on generating tokens for dynamic regions. This design reduces the total number of tokens while lowering the computational cost for subsequent transformer modeling:

$$\begin{aligned} \mathbf{Z}_t^d &= \mathcal{E}_p(\mathbf{O}_t | \mathbf{O}_{1:T_0}), \\ \hat{\mathbf{O}}_t &= \mathcal{D}_c(\mathbf{Z}_t^d | \mathbf{O}_{1:T_0}), \quad t = T_0 + 1, \dots, T \end{aligned} \quad (2)$$

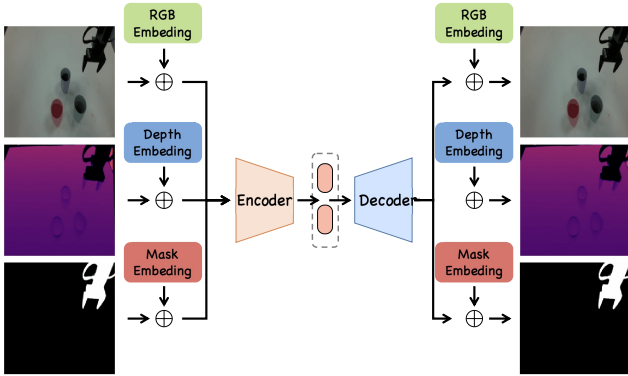


Fig. 3: **Overview of MMTokenizer.** We introduce MMTokenizer to generate unified tokens from multi-modal inputs, which not only reduces computational cost but also incorporates geometric information into the tokens, enhancing the capabilities of iMoWM. Specifically, we repeat the first and last layers of the original VAE and combine different embeddings to mitigate distributional differences across modalities.

The conditioning mechanism is implemented through cross-attention between the context tokens and future observations, enabling selective modeling of scene dynamics.

We train MMTokenizer following the original VQGAN framework, with an objective defined as:

$$\mathcal{L}_{\text{tokenizer}} = \sum_{t=1}^{T_0} \mathcal{L}_{\text{VQGAN}}(\mathbf{O}_t; \mathcal{E}_c, \mathcal{D}_c) + \sum_{t=T_0+1}^T \mathcal{L}_{\text{VQGAN}}(\mathbf{O}_t; \mathcal{E}_d, \mathcal{D}_d) \quad (3)$$

where  $\mathcal{L}_{\text{VQGAN}}$  comprises an  $\mathcal{L}_1$  reconstruction loss, a commitment loss [45], a perceptual loss [46], and optionally an adversarial loss [44].

### B. Autoregressive Transformer

With the above MMTokenizer, the multi-modal video inputs are flattened into sequences of context and dynamic tokens,  $\{\mathbf{Z}_t^c\}_{t=1}^{T_0}, \{\mathbf{Z}_t^d\}_{t=T_0+1}^T$ . Then, for efficient training, we follow [12] to construct the token sequence  $\mathbf{X}_T = (\mathbf{Z}_1^c, [\mathbf{S}_1], \mathbf{Z}_2^c, \dots, \mathbf{Z}_{T_0}^c, [\mathbf{S}_{T_0}], \mathbf{Z}_{T_0+1}^d, [\mathbf{S}_{T_0+1}], \dots, \mathbf{Z}_T^d)$ . As illustrated in Figure 2, we introduce a slot token  $[\mathbf{S}_a]$  to delimit observations and inject action conditioning:

$$[\mathbf{S}_t] = [\mathbf{S}] + \text{Linear}(\mathbf{a}_t) \quad (4)$$

Here,  $[\mathbf{S}]$  is a unified boundary flag with a fixed maximum value, and  $\mathbf{a}_t$  denotes the end-effector pose, including position, orientation, and gripper state. We project actions into the model latent space using a simple linear network to obtain an action embedding. Using the unified multi-modal token representation, we adopt a LLaMA-style [47] transformer architecture with RMSNorm [48], SwiGLU activation [49], and rotary positional embeddings [50], initialized from pretrained checkpoints [12]. The transformer is trained to predict next

tokens using a cross-entropy objective:

$$\mathcal{L}_{\text{transformer}} = - \sum_{t=T_0+1}^T \log(\mathbf{X}_t | \mathbf{X}_{t-1}) \quad (5)$$

where  $\mathbf{X}_t$  denotes the token sequence up to the current time step. Consistent with our token-efficiency design, we compute the loss only over dynamic tokens (those encoding scene changes) and context tokens are excluded from the transformer loss. To simplify batching and align context regions across examples, we pad with empty tokens  $[\mathbf{E}]$ . At inference time, future tokens are generated autoregressively and previously generated tokens are fed back as conditions for subsequent steps.

### C. Downstream Tasks

**iMoWM for Imitation Learning.** World models are capable of predicting future observations conditioned on actions, thereby serving as a powerful form of data augmentation for real-world data. In our framework, we employ iMoWM to roll out multiple demonstrations given an initial observation and a successful action sequence. The generated multi-modal outputs are then utilized to train a robotic manipulation policy via 3D Diffusion Policy [35]. For our imitation learning setup, we use only color images and depth maps as inputs to the policy, while actions are predicted in sequential chunks to ensure temporal consistency in robotic control.

**iMoWM for Reinforcement Learning.** Similar to other world model approaches [12], [9], iMoWM can readily serve as an imagined simulator within existing model-based RL frameworks. The objective of model-based RL [51] is to learn a policy  $\pi$  that maximizes the cumulative reward  $\mathbf{r}$  through policy roll-outs. We formalize this as a Markov Decision Process (MDP) defined by  $(\mathbf{S}, \mathbf{A}, \mathcal{P}, \mathbf{r}, \gamma)$ , where  $\mathbf{S}$  and  $\mathbf{A}$  denote the state and action spaces,  $\mathcal{P}$  represents the world model that predicts state transitions, and  $\gamma$  is the discount factor. We first construct a real replay buffer  $\mathcal{D}_{\text{real}}$  using an initialized policy  $\pi$  and train iMoWM  $\mathcal{P}_\theta$  on  $\mathcal{D}_{\text{real}}$ . Subsequently,  $\mathcal{P}_\theta$  is employed to generate an imagined replay buffer  $\mathcal{D}_{\text{imag}}$  under the same action roll-outs. The actor-critic model  $(\pi, v)$  is then updated using the combined dataset  $\mathcal{D}_{\text{real}} \cup \mathcal{D}_{\text{imag}}$ . In addition, we incorporate an auxiliary reward head to predict the reward for each action step, following [12].

## IV. EXPERIMENTS

In this section, we compare iMoWM with prior state-of-the-art methods across three robotic manipulation tasks. We first demonstrate its superior visual quality and depth accuracy for action-conditioned multi-modal video generation in section IV-A. Next, we evaluate visual model-based RL performance in simulator, as presented in section IV-B. To further substantiate the quality of our roll-out multi-modal video sequences, we conduct real-world imitation learning experiments in section IV-C. Finally, we analyze the contributions of the proposed MMTokenizer and assess the efficiency of our multi-modal design in section IV-D.

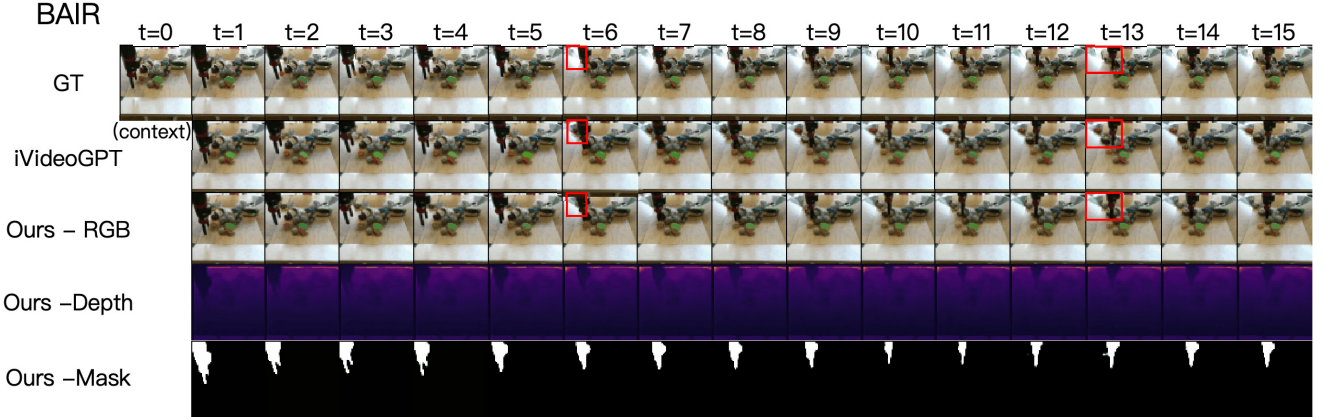


Fig. 4: **Comparisons on BAIR dataset.** We present action-conditioned multi-modal video generation results on the BAIR dataset, comparing with iVideoGPT. Our method produces better generations and captures richer geometric information.

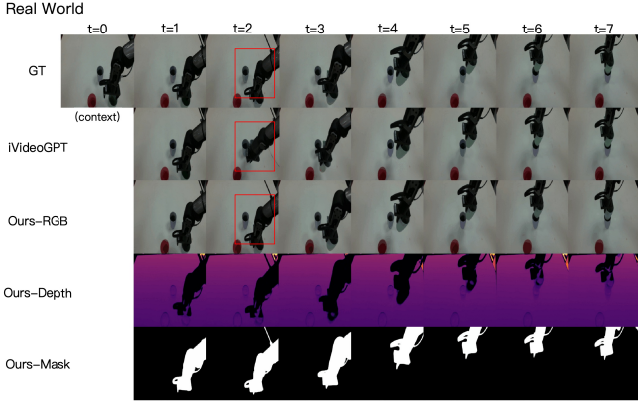


Fig. 5: **Comparison on real data.** We showcase qualitative results on real-world, high-resolution data. The results demonstrate the superiority of iMoWM in controllable multi-modal video generation with interaction.

Additional videos and implementation details of iMoWM are provided in the supplementary material.

#### A. Action-conditioned Multi-modal Video Generation

We evaluate iMoWM on the action-conditioned multi-modal video generation task using the BAIR robot pushing dataset [18] (43k training videos and 256 testing videos) and the RoboNet dataset [19] (162k videos collected across seven robotic arms). To reduce computational overhead, we use a subset of 19k training videos and 256 testing videos from RoboNet, corresponding to the same robotic arm. For multi-modal inputs, we generate metric depth maps using Video Depth Anything [54] and obtain temporally consistent robot-arm masks with Grounding DINO [55] and SAM2 [56]. Both datasets are provided at a resolution of  $64 \times 64$ . For high-resolution experiments, we additionally use a self-collected dataset consisting of 1k training videos and 150 test videos spanning six robotic manipulation tasks at a resolution of  $256 \times 256$ . We compare iMoWM against open-source baselines, including MaskViT [2], SVG [52], GHVAE [53], and iVideoGPT [12]. For visual quality, we report FVD [57],

BAIR[18]	FVD↓	PSNR↑	SSIM↑	LPIPS↓	AbsRel↓
MaskViT[2]	70.5	-	-	-	-
iVideoGPT[12]	<u>65.01</u>	23.40	<u>0.882</u>	0.058	0.059
<b>Ours</b>	<b>60.9</b>	<b>23.82</b>	<b>0.896</b>	<b>0.051</b>	<b>0.045</b>
RoboNet[19]	FVD↓	PSNR↑	SSIM↑	LPIPS↓	AbsRel↓
MaskViT[2]	133.5	23.2	0.805	0.042	-
SVG[52]	123.2	23.9	0.878	0.060	-
GHVAE[53]	95.2	24.7	0.891	<u>0.036</u>	-
iVideoGPT[12]	<b>65.8</b>	<u>27.2</u>	<u>0.895</u>	0.053	<u>0.054</u>
<b>Ours</b>	<u>67.6</u>	<b>28.0</b>	<b>0.920</b>	<b>0.032</b>	<b>0.031</b>

TABLE I: **Quantitative comparisons on BAIR and RoboNet dataset.** Our results outperform iVideoGPT across all metrics on both datasets, demonstrating the effectiveness of the proposed multi-modal world model for future generation. (**Bold** figures indicate the best, and underlined figures indicate the second-best.)

PSNR [58], SSIM [59], and LPIPS [60] scores. For depth accuracy, we adopt the AbsRel metric (absolute relative error:  $\frac{|d-d|}{d}$ ) [61]. To ensure fairness, we generate four roll-outs for both iVideoGPT and our method. For other baselines, we use Video Depth Anything to generate depth maps from their roll-outs in order to compute depth metrics.

The results are presented in Table I. Our method outperforms all baselines on the BAIR dataset in both visual and depth quality, demonstrating that the multi-modal world model enhances performance by providing a better understanding of the physical world. On the RoboNet dataset, iMoWM achieves superior performance on most metrics, benefiting from the explicit incorporation of depth for enhanced geometric representation. iVideoGPT obtains a better FVD score, largely due to pretraining on 162K training videos—a significantly larger dataset. Our results on RoboNet surpass those on BAIR, as RoboNet provides higher-resolution data that allows for more accurate multi-modal annotations. We further evaluate iMoWM on high-resolution real-world data with input from a depth sensor. The quantitative results in Table II highlight that iMoWM achieves stronger performance with higher-resolution inputs, as richer 3D information is incorporated. Qualitative results

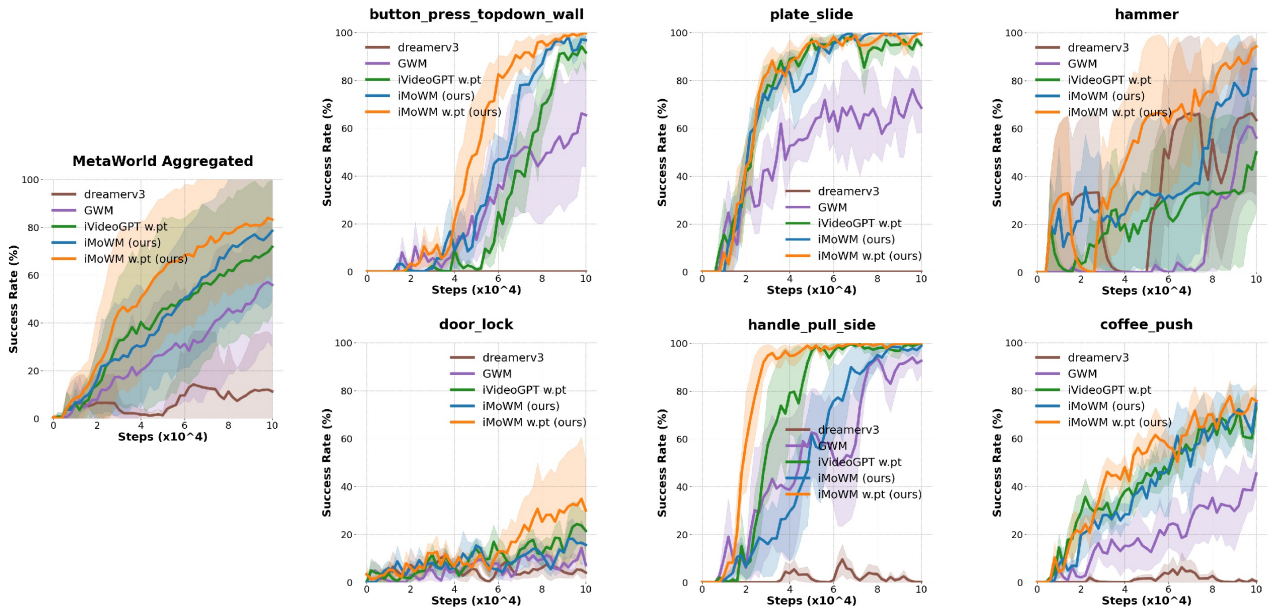


Fig. 6: **MBRL Results on Metaworld.** The shaded region indicates the 95% confidence interval (CI) across three random seeds, with each data point evaluated over 20 episodes. The results demonstrate that iMoWM exhibits a stronger understanding of the physical world and improves both the convergence speed and accuracy of reinforcement learning methods.

Real-world	PSNR $\uparrow$	SSIM $\uparrow$	LPIPS $\downarrow$
iVideoGPT [12]	33.24	0.914	0.138
<b>Ours</b>	<b>38.33</b>	<b>0.954</b>	<b>0.097</b>

TABLE II: **Quantitative comparisons on real data.** We compare our method against iVideoGPT on real-world data at a resolution of  $256 \times 256$ . Our method outperforms the previous SOTA at higher resolution, highlighting the potential of iMoWM, as increased resolution provides more detailed depth maps and more precise robot-arm masks.

A1 Arm	iVideoGPT	Ours	GT
Stack First Cup	5 / 10	<b>9 / 10</b>	9 / 10
Stack Second Cup	3 / 10	<b>7 / 10</b>	6 / 10
Pick and Place	7 / 15	<b>13 / 15</b>	12 / 15
Total	13 / 35	<b>29 / 35</b>	27 / 35

TABLE III: **Real-world deploy experiment results.** We evaluate our method on two real-world tasks: stacking two cups and picking bread to a basket. The first longer task is divided into two key subtasks, while for the pick-and-place task, we introduce positional distractors for both the bread and the basket. The results demonstrate that iMoWM roll-outs can serve as real-world data for policy training.

on the BAIR dataset and real-world data, shown in Figure 4 and Figure 5, further demonstrate the superiority of iMoWM in action-conditioned video generation tasks.

### B. Visual Model-based RL

We evaluate the performance of iMoWM for RL learning on six robotic manipulation tasks from the Meta-World benchmark [20]. Our approach employs a model-based RL framework inspired by MBPO [51], using DrQ-v2 [62] as

the actor-critic algorithm. To ensure fair comparisons, all compared methods are trained under identical settings, with iVideoGPT [12] initialized from pretrained checkpoints.

Figure 6 demonstrates that iMoWM outperforms all baselines across the six Meta-World tasks. On average, iMoWM converges faster than both iVideoGPT and GWM, and ultimately achieves higher success rates on both simple and complex tasks. This performance improvement can be attributed to the geometry-aware roll-outs of our world model, in contrast to purely image-based approaches. Moreover, iMoWM surpasses 3DGS-based GWM indicating that depth-map prediction provides a more efficient representation for modular environments such as those in Meta-World.

### C. Real world Imitation Learning

We further evaluate the quality of iMoWM roll-outs through real-world deployment experiments. A GALAXEA A1 robotic arm is used for these experiments, with a third-view Realsense D435i camera providing RGB-D observations. We collect a small dataset of 50 demonstrations for the pickup-bread-to-basket and stack-two-cups tasks. Using the pre-trained iMoWM described in section IV-A, we generate 50 imagined trajectories conditioned on the actions in these demonstrations. The imagined data from iVideoGPT (combined with GT depths), iMoWM, and the collected real demonstrations are used to train a 3D Diffusion Policy [35]. The results, presented in Table III, compare task success rates to provide a quantitative assessment of rollout quality. We decompose the long-horizon task into key subtasks and evaluate each method under position distractors for both the bread and basket. Our method achieves performance comparable to ground-truth data, demonstrating the high fidelity of our multi-modal rollouts.

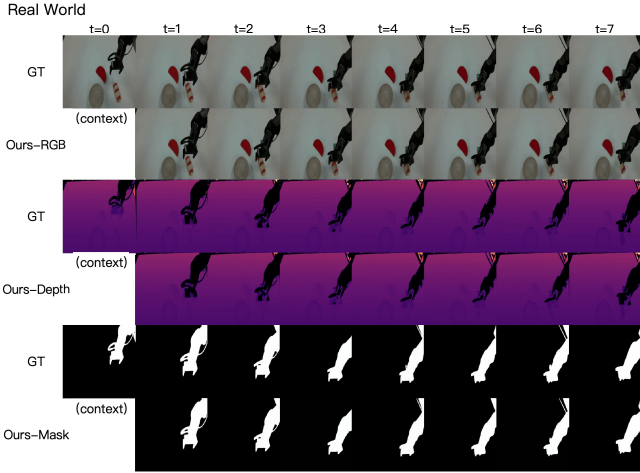


Fig. 7: **Qualitative Result on Real Data.** We present qualitative results on real-world, high-resolution data and multi-modal ground-truth.

BAIR[18]	FVD↓	PSNR↑	SSIM↑	LPIPS↓	Infer. Time
original	739.2	16.64	0.735	0.176	860s
<b>MMTokenizer</b>	<b>67.6</b>	<b>23.22</b>	<b>0.885</b>	<b>0.056</b>	<b>10s</b>
RGB	70.2	22.50	0.865	0.066	-
RGB+Mask	70.6	22.84	0.877	0.059	-
RGB+Depth	<b>67.5</b>	22.67	0.873	0.061	-
<b>Ours</b>	67.6	<b>23.22</b>	<b>0.885</b>	<b>0.056</b>	-

TABLE IV: **Ablation study on BAIR dataset.** We conduct an ablation study on MMTokenizer and multi-modal observations. The results demonstrate the superiority of both components of our proposed method.

#### D. Ablation Study

We conduct ablation experiments on the BAIR dataset [18] to further demonstrate the advantages of our MMTokenizer and multi-modal world model. All these ablation experiments use same training storage and are inferenced on a single RTX 3090 GPU. The results are reported in Table IV, where MMTokenizer is compared against the original tokenizer that employs three times more tokens in the transformer network. The findings highlight the importance of MMTokenizer in both accelerating generation and improving convergence speed. Furthermore, we evaluate the contribution of each modality independently. The results show that every modality enhances overall performance by providing geometric information or dynamic attention.

#### V. CONCLUSION

In this work, we introduce iMoWM, a novel interactive multi-modal world model designed for robotic manipulation tasks. Our method focuses on incorporating geometric information and dynamic attention mechanisms to enhance world model performance. To achieve efficient representation, we propose MMTokenizer, which encodes multi-modal observations into unified tokens, and employ an autoregressive transformer to generate future states conditioned on actions. We conduct extensive experiments demonstrating both the

visual quality improvements of our video generation results and their benefits for downstream robotic manipulation tasks, including reinforcement learning and imitation learning. Nevertheless, large-scale pretraining remains necessary for iMoWM to fully realize the generalizability of multi-modal world models with various robot arms and action conditions.

#### REFERENCES

- [1] A. Bar, G. Zhou, D. Tran, T. Darrell, and Y. LeCun, "Navigation world models," in *Proceedings of the Computer Vision and Pattern Recognition Conference (CVPR)*, 2025, pp. 15 791–15 801.
- [2] A. Gupta, S. Tian, Y. Zhang, J. Wu, R. Martín-Martín, and L. Fei-Fei, "Maskvit: Masked visual pre-training for video prediction," *arXiv preprint arXiv:2206.11894*, 2022.
- [3] H. Liang, J. Cao, V. Goel, G. Qian, S. Korolev, D. Terzopoulos, K. N. Plataniotis, S. Tulyakov, and J. Ren, "Wonderland: Navigating 3d scenes from a single image," in *Proceedings of the Computer Vision and Pattern Recognition Conference (CVPR)*, 2025, pp. 798–810.
- [4] C. D. Singh, R. Kumari, C. Fermüller, N. J. Sanket, and Y. Aloimonos, "Worldgen: A large scale generative simulator," in *2023 IEEE International Conference on Robotics and Automation (ICRA)*. IEEE, 2023, pp. 9147–9154.
- [5] Y. Zou, Y. Ding, C. Zhang, J. Guo, B. Li, X. Lyu, F. Tan, X. Qi, and H. Wang, "Mudg: Taming multi-modal diffusion with gaussian splatting for urban scene reconstruction," *arXiv preprint arXiv:2503.10604*, 2025.
- [6] S. Zuo, W. Zheng, Y. Huang, J. Zhou, and J. Lu, "Gaussianworld: Gaussian world model for streaming 3d occupancy prediction," in *Proceedings of the Computer Vision and Pattern Recognition Conference (CVPR)*, 2025, pp. 6772–6781.
- [7] X. Cheng, T. He, J. Xu, J. Guo, D. He, and J. Bian, "Playing with transformer at 30+ fps via next-frame diffusion," *arXiv preprint arXiv:2506.01380*, 2025.
- [8] D. Hafner, J. Pasukonis, J. Ba, and T. Lillicrap, "Mastering diverse domains through world models," *arXiv preprint arXiv:2301.04104*, 2023.
- [9] G. Lu, B. Jia, P. Li, Y. Chen, Z. Wang, Y. Tang, and S. Huang, "Gwm: Towards scalable gaussian world models for robotic manipulation," *arXiv preprint arXiv:2508.17600*, 2025.
- [10] C. Zhang, Y. Ling, M. Lu, M. Qin, and H. Wang, "Category-level object detection, pose estimation and reconstruction from stereo images," in *European Conference on Computer Vision*. Springer, 2024, pp. 332–349.
- [11] H. Zhen, Q. Sun, H. Zhang, J. Li, S. Zhou, Y. Du, and C. Gan, "Tesseract: learning 4d embodied world models," *arXiv preprint arXiv:2504.20995*, 2025.
- [12] J. Wu, S. Yin, N. Feng, X. He, D. Li, J. Hao, and M. Long, "ivideoqpt: Interactive videoqpts are scalable world models," *Advances in Neural Information Processing Systems*, vol. 37, pp. 68 082–68 119, 2024.
- [13] W. Hong, M. Ding, W. Zheng, X. Liu, and J. Tang, "Cogvideo: Large-scale pretraining for text-to-video generation via transformers," *arXiv preprint arXiv:2205.15868*, 2022.
- [14] T. Wan, A. Wang, B. Ai, B. Wen, C. Mao, C.-W. Xie, D. Chen, F. Yu, H. Zhao, J. Yang *et al.*, "Wan: Open and advanced large-scale video generative models," *arXiv preprint arXiv:2503.20314*, 2025.
- [15] X. Guo, Y. Zhang, B. Chen, H. Xu, J. Wang, and M. Long, "Dynamical diffusion: Learning temporal dynamics with diffusion models," *arXiv preprint arXiv:2503.00951*, 2025.
- [16] J. Cen, C. Yu, H. Yuan, Y. Jiang, S. Huang, J. Guo, X. Li, Y. Song, H. Luo, F. Wang *et al.*, "Worldvla: Towards autoregressive action world model," *arXiv preprint arXiv:2506.21539*, 2025.
- [17] B. Kerbl, G. Kopanas, T. Leimkühler, and G. Drettakis, "3d gaussian splatting for real-time radiance field rendering," *ACM Transactions on Graphics*, vol. 42, no. 4, July 2023.
- [18] F. Ebert, C. Finn, A. X. Lee, and S. Levine, "Self-supervised visual planning with temporal skip connections," *CoRL*, vol. 12, no. 16, p. 23, 2017.
- [19] S. Dasari, F. Ebert, S. Tian, S. Nair, B. Bucher, K. Schmeckpeper, S. Singh, S. Levine, and C. Finn, "Robonet: Large-scale multi-robot learning," *arXiv preprint arXiv:1910.11215*, 2019.

- [20] T. Yu, D. Quillen, Z. He, R. Julian, K. Hausman, C. Finn, and S. Levine, "Meta-world: A benchmark and evaluation for multi-task and meta reinforcement learning," in *Conference on robot learning*. PMLR, 2020, pp. 1094–1100.
- [21] W. Zheng, W. Chen, Y. Huang, B. Zhang, Y. Duan, and J. Lu, "Occworld: Learning a 3d occupancy world model for autonomous driving," in *European conference on computer vision*. Springer, 2024, pp. 55–72.
- [22] X. Wang, Z. Zhu, G. Huang, X. Chen, J. Zhu, and J. Lu, "Drive-dreamer: Towards real-world-drive world models for autonomous driving," in *European conference on computer vision*. Springer, 2024, pp. 55–72.
- [23] B. Li, J. Guo, H. Liu, Y. Zou, Y. Ding, X. Chen, H. Zhu, F. Tan, C. Zhang, T. Wang *et al.*, "Uniscene: Unified occupancy-centric driving scene generation," in *Proceedings of the Computer Vision and Pattern Recognition Conference (CVPR)*, 2025, pp. 11 971–11 981.
- [24] Z. Li, X. Xu, Z. Xu, S. Lim, and H. Zhao, "Larm: Large autoregressive model for long-horizon embodied intelligence," *arXiv preprint arXiv:2405.17424*, 2024.
- [25] W. Ye, S. Liu, T. Kurutach, P. Abbeel, and Y. Gao, "Mastering atari games with limited data," *Advances in neural information processing systems*, vol. 34, pp. 25 476–25 488, 2021.
- [26] J. Schrittwieser, I. Antonoglou, T. Hubert, K. Simonyan, L. Sifre, S. Schmitt, A. Guez, E. Lockhart, D. Hassabis, T. Graepel *et al.*, "Mastering atari, go, chess and shogi by planning with a learned model," *Nature*, vol. 588, no. 7839, pp. 604–609, 2020.
- [27] Y. Seo, D. Hafner, H. Liu, F. Liu, S. James, K. Lee, and P. Abbeel, "Masked world models for visual control," in *Conference on Robot Learning*. PMLR, 2023, pp. 1332–1344.
- [28] P. Wu, A. Escontrela, D. Hafner, P. Abbeel, and K. Goldberg, "Day-dreamer: World models for physical robot learning," in *Conference on robot learning*. PMLR, 2023, pp. 2226–2240.
- [29] N. Hansen, H. Su, and X. Wang, "Td-mpc2: Scalable, robust world models for continuous control," *arXiv preprint arXiv:2310.16828*, 2023.
- [30] D. Kondratyuk, L. Yu, X. Gu, J. Lezama, J. Huang, G. Schindler, R. Hornung, V. Birodkar, J. Yan, M.-C. Chiu *et al.*, "Videopoet: A large language model for zero-shot video generation," *arXiv preprint arXiv:2312.14125*, 2023.
- [31] R. Wu, R. Gao, B. Poole, A. Trevithick, C. Zheng, J. T. Barron, and A. Holynski, "Cat4d: Create anything in 4d with multi-view video diffusion models," in *Proceedings of the Computer Vision and Pattern Recognition Conference (CVPR)*, 2025, pp. 26 057–26 068.
- [32] Y. Yin, D. Xu, Z. Wang, Y. Zhao, and Y. Wei, "4dgen: Grounded 4d content generation with spatial-temporal consistency," *arXiv preprint arXiv:2312.17225*, 2023.
- [33] U. Singer, S. Sheynin, A. Polyak, O. Ashual, I. Makarov, F. Kokkinos, N. Goyal, A. Vedaldi, D. Parikh, J. Johnson *et al.*, "Text-to-4d dynamic scene generation," *arXiv preprint arXiv:2301.11280*, 2023.
- [34] J. Ren, L. Pan, J. Tang, C. Zhang, A. Cao, G. Zeng, and Z. Liu, "Dreamgaussian4d: Generative 4d gaussian splatting," *arXiv preprint arXiv:2312.17142*, 2023.
- [35] C. Chi, Z. Xu, S. Feng, E. Cousineau, Y. Du, B. Burchfiel, R. Tedrake, and S. Song, "Diffusion policy: Visuomotor policy learning via action diffusion," *The International Journal of Robotics Research*, p. 02783649241273668, 2023.
- [36] Y. Ze, G. Zhang, K. Zhang, C. Hu, M. Wang, and H. Xu, "3d diffusion policy: Generalizable visuomotor policy learning via simple 3d representations," *arXiv preprint arXiv:2403.03954*, 2024.
- [37] M. J. Kim, K. Pertsch, S. Karamcheti, T. Xiao, A. Balakrishna, S. Nair, R. Rafailov, E. Foster, G. Lam, P. Sanketi *et al.*, "Openvla: An open-source vision-language-action model," *arXiv preprint arXiv:2406.09246*, 2024.
- [38] P. Li, Y. Wu, Z. Xi, W. Li, Y. Huang, Z. Zhang, Y. Chen, J. Wang, S.-C. Zhu, T. Liu *et al.*, "Controlvla: Few-shot object-centric adaptation for pre-trained vision-language-action models," *arXiv preprint arXiv:2506.16211*, 2025.
- [39] J. Luo, Z. Hu, C. Xu, Y. L. Tan, J. Berg, A. Sharma, S. Schaal, C. Finn, A. Gupta, and S. Levine, "Serl: A software suite for sample-efficient robotic reinforcement learning," in *2024 IEEE International Conference on Robotics and Automation (ICRA)*. IEEE, 2024, pp. 16 961–16 969.
- [40] J. Luo, C. Xu, J. Wu, and S. Levine, "Precise and dexterous robotic manipulation via human-in-the-loop reinforcement learning," *Science Robotics*, vol. 10, no. 105, p. eads5033, 2025.
- [41] M. Okada and T. Taniguchi, "Dreamingv2: Reinforcement learning with discrete world models without reconstruction," in *2022 IEEE/RSJ International Conference on Intelligent Robots and Systems (IROS)*. IEEE, 2022, pp. 985–991.
- [42] J. Achiam, S. Adler, S. Agarwal, L. Ahmad, I. Akkaya, F. L. Aleman, D. Almeida, J. Altenschmidt, S. Altman, S. Anadkat *et al.*, "Gpt-4 technical report," *arXiv preprint arXiv:2303.08774*, 2023.
- [43] D. Lee, C. Kim, S. Kim, M. Cho, and W.-S. Han, "Autoregressive image generation using residual quantization," in *Proceedings of the Computer Vision and Pattern Recognition Conference (CVPR)*, 2022, pp. 11 523–11 532.
- [44] P. Esser, R. Rombach, and B. Ommer, "Taming transformers for high-resolution image synthesis," in *Proceedings of the Computer Vision and Pattern Recognition Conference (CVPR)*, 2021, pp. 12 873–12 883.
- [45] A. Van Den Oord, O. Vinyals *et al.*, "Neural discrete representation learning," *Advances in neural information processing systems*, vol. 30, 2017.
- [46] J. Johnson, A. Alahi, and L. Fei-Fei, "Perceptual losses for real-time style transfer and super-resolution," in *European conference on computer vision*. Springer, 2016, pp. 694–711.
- [47] H. Touvron, L. Martin, K. Stone, P. Albert, A. Almahairi, Y. Babaei, N. Bashlykov, S. Batra, P. Bhargava, S. Bhosale *et al.*, "Llama 2: Open foundation and fine-tuned chat models," *arXiv preprint arXiv:2307.09288*, 2023.
- [48] B. Zhang and R. Sennrich, "Root mean square layer normalization," *Advances in neural information processing systems*, vol. 32, 2019.
- [49] N. Shazeer, "Glu variants improve transformer," *arXiv preprint arXiv:2002.05202*, 2020.
- [50] J. Su, M. Ahmed, Y. Lu, S. Pan, W. Bo, and Y. Liu, "Roformer: Enhanced transformer with rotary position embedding," *Neurocomputing*, vol. 568, p. 127063, 2024.
- [51] M. Janner, J. Fu, M. Zhang, and S. Levine, "When to trust your model: Model-based policy optimization," *Advances in neural information processing systems*, vol. 32, 2019.
- [52] R. Villegas, A. Pathak, H. Kannan, D. Erhan, Q. V. Le, and H. Lee, "High fidelity video prediction with large stochastic recurrent neural networks," *Advances in Neural Information Processing Systems*, vol. 32, 2019.
- [53] B. Wu, S. Nair, R. Martin-Martin, L. Fei-Fei, and C. Finn, "Greedy hierarchical variational autoencoders for large-scale video prediction," in *Proceedings of the Computer Vision and Pattern Recognition Conference (CVPR)*, 2021, pp. 2318–2328.
- [54] S. Chen, H. Guo, S. Zhu, F. Zhang, Z. Huang, J. Feng, and B. Kang, "Video depth anything: Consistent depth estimation for super-long videos," in *Proceedings of the Computer Vision and Pattern Recognition Conference (CVPR)*, 2025, pp. 22 831–22 840.
- [55] S. Liu, Z. Zeng, T. Ren, F. Li, H. Zhang, J. Yang, Q. Jiang, C. Li, J. Yang, H. Su *et al.*, "Grounding dino: Marrying dino with grounded pre-training for open-set object detection," in *European conference on computer vision*. Springer, 2024, pp. 38–55.
- [56] N. Ravi, V. Gabeur, Y.-T. Hu, R. Hu, C. Ryal, T. Ma, H. Khedr, R. Rädle, C. Rolland, L. Gustafson *et al.*, "Sam 2: Segment anything in images and videos," *arXiv preprint arXiv:2408.00714*, 2024.
- [57] T. Unterthiner, S. Van Steenkiste, K. Kurach, R. Marinier, M. Michalski, and S. Gelly, "Towards accurate generative models of video: A new metric & challenges," *arXiv preprint arXiv:1812.01717*, 2018.
- [58] Q. Huynh-Thu and M. Ghanbari, "Scope of validity of psnr in image/video quality assessment," *Electronics letters*, vol. 44, no. 13, pp. 800–801, 2008.
- [59] Z. Wang, A. C. Bovik, H. R. Sheikh, and E. P. Simoncelli, "Image quality assessment: from error visibility to structural similarity," *IEEE transactions on image processing*, vol. 13, no. 4, pp. 600–612, 2004.
- [60] R. Zhang, P. Isola, A. A. Efros, E. Shechtman, and O. Wang, "The unreasonable effectiveness of deep features as a perceptual metric," in *Proceedings of the Computer Vision and Pattern Recognition Conference (CVPR)*, 2018, pp. 586–595.
- [61] L. Yang, B. Kang, Z. Huang, X. Xu, J. Feng, and H. Zhao, "Depth anything: Unleashing the power of large-scale unlabeled data," in *Proceedings of the Computer Vision and Pattern Recognition Conference (CVPR)*, 2024, pp. 10 371–10 381.
- [62] D. Yarats, R. Fergus, A. Lazaric, and L. Pinto, "Mastering visual continuous control: Improved data-augmented reinforcement learning," *arXiv preprint arXiv:2107.09645*, 2021.